International Journal of Heat and Mass Transfer 52 (2009) 880–893

Contents lists available at ScienceDirect

International Journal of Heat and Mass Transfer

journal homepage: www.elsevier.com/locate/ijhmt

Heat transfer in tilted reciprocating anti-gravity open thermosyphon

Tsun Lirng Yang [a], Shyy Woei Chang [b,*]

[a] Department of Marine Engineering, National Kaohsiung Marine University, No. 142, Haijhuan Road, Nanzih District, Kaohsiung 811, Taiwan, ROC
[b] Thermal Fluids Laboratory, Department of Marine Engineering, National Kaohsiung Marine University, No. 142, Haijhuan Road, Nanzih District, Kaohsiung 811, Taiwan, ROC

ARTICLE INFO

Article history:
Received 8 October 2007
Received in revised form 11 July 2008
Available online 26 August 2008

Keywords:
Open thermosyphon
Reciprocating flow
Piston cooling

ABSTRACT

This experimental study generates a new set of Nusselt number (*Nu*) data from two opposite upper and lower edges of a tilted reciprocating anti-gravity open tubular thermosyphon that emulates closely the realistic '*shaker-bored*' cooling conditions inside a piston of marine propulsive diesel engine. The impacts of thermosyphon inclination on heat transfer are described by way of comparisons between two sets of *Nu* data generated from the vertical and tilted reciprocating thermosyphons. Nusselt number differences between two opposite upper (Nu_{Upper}) and lower (Nu_{Lower}) edges along the tilted thermosyphon are amplified as the reciprocating force increases; while no appreciable differences between Nu_{Upper} and Nu_{Lower} are observed in the *tilted static* thermosyphon or in the *vertical* static and reciprocating thermosyphon. For such tilted reciprocating open thermosyphon, the individual and interactive influences of inertial, reciprocating and buoyancy forces on heat transfer are described for both sub-cooled (single phase) and superheated (two phase) conditions. Due to the synergistic effects of inertial force, reciprocating force and buoyancy interactions for all the experimental conditions tested, the worst heat transfer scenarios in terms of the axially averaged *Nu* values in the *tilted reciprocating open thermosyphon* fall to the level of 0.82 times of the static levels. A set of empirical heat transfer correlations which permits the evaluation of axially averaged Nusselt numbers is developed to assist the design activity of such piston cooling system.

1. Introduction

Internal cooling networks are essential to avoid thermal damages on pistons in a heavy-duty marine propulsive diesel engine. This class of diesel engine is running at low speeds ranging from 90 to 120 rev/min with the larger than normal stroke-to-bore ratio. Coolant flows inside the cooling network of a piston thus reciprocate at low frequencies. A typical piston cooling network, which is referred to as the multi-bore shaker cooling system, along with the flow structures inside its vertical blind bore are depicted in Fig. 1. Here, the coolant, treated water or lubricating oil, in each blind bore is shaken "from" and "to" the plenum chamber when the piston reciprocates. The plenum chamber acts as a heat-sink reservoir in which the hot coolant from each blind bore is mixed with the cold coolant fed from the telescopic pipe. Heat fluxes conducted from the piston are convected out of each blind bore by way of vortical transportations [1,2]. But the wall temperatures along each blind bore increase in the opposite direction of earth gravity. Such a flow configuration is the so-called anti-gravity open thermosyphon [3] which is rarely investigated before. Depending on the material temperatures of the piston, the coolant flows in these blind bores are sub-cooled and/or superheated. Also there is no net mass flow rate across any cross-sectional plane of the blind channel. As a result, the flow structure in such long blind channel can be developed as several coherent counter-rotating vortical cells or as the counter-directional hot and cold streams. As indicated in Fig. 1b for a vertical reciprocating blind bore [2], the largest and strongest vortical cell locates at the immediate open entrance that is induced by the cross flow over the open-end of the blind bore. Several tube-wise vortical cells with weaker strengths are sequentially induced by their upstream vortices in the counter-rotating manners. At the flow region adjoining the sealed end of the coolant channel, buoyancy effects dominate the regional thermal fluid phenomena [1]. Acting by the buoyancy forces alone, the heated wall-flows are directed toward the sealed end of the blind bore. These heated wall-flows are confluent at the blind central and then directed toward the bottom end to preserve the mass continuity of coolant flows. Fig. 1b depicts the conceptual flow structures in a vertical reciprocating anti-gravity open thermosyphon which are reconstructed from the LDV measurements [2]. It is noticed that the strengths and structures for the pair of stretched vortices at the top region of the vertical open thermosyphon depend greatly on the buoyancy levels and the thermal boundary condition imposed. For any form of thermal boundary with asymmetric wall temperature distributions around its channel perimeter, the pair of longitudinal vortices adjacent to the sealed end of thermosyphon becomes three dimensional.

* Corresponding author. Tel.: +886 76126256; fax: +886 73629500.
E-mail address: swchang@mail.nkmu.edu.tw (S.W. Chang).

0017-9310/$ - see front matter © 2008 Elsevier Ltd. All rights reserved.
doi:10.1016/j.ijheatmasstransfer.2008.07.014

Nomenclature

a_s, b_s	Functional coefficients
d	Internal diameter of thermosyphon tube (m)
f_R	Reciprocating frequency (Hz)
Gr_g	Gravitational Grashof number = $g\beta\,(T_w - T_f)d^3/\upsilon^2$
Gr_p	Pulsating Grashof number = $\omega^2 R\beta(T_w - T_f)d^3/\upsilon^2$
k_f	Thermal conductivity of coolant ($Wm^{-1}\,K^{-1}$)
L	Length of thermosyphon tube (m)
$\dot{m}$	Coolant mass flow rate ($kg\,s^{-1}$)
Nu	Nusselt number = $q_f d/(T_w - T_f)k_f$
$\overline{Nu}$	Averaged Nusselt number
Pr	Prandtl number = $\mu C_p/k_f$
Pu	Pulsating number = $\omega d/W_m$ (pulsating-to-inertial force ratio)
q_f	Local heat flux (Wm^{-2})
R	Reciprocating amplitude (m)
Re	Reynolds number = $4\dot{m}/(\pi d\mu)$
S	Stroke of the reciprocating test rig = $2R$ (m)
T_f	Reference fluid temperature at the entrance of thermosyphon tube (K)
T_{sat}	Saturated fluid temperature (K)
T_w	Wall temperature (K)
ΔT_f	Fluid temperature rise through heat transfer test module (K)
W_m	Characteristic flow velocity = $\dot{m}/\rho d^2$ (ms^{-1})
X	Axial coordinate (m)

Greek symbols

α	Tilting angle of thermosyphon tube (degree)
μ	Dynamic viscosity of coolant ($kg\,m^{-1}\,s^{-1}$)
ω	Angular velocity of rotating disc creating reciprocating motion ($rads^{-1}$)
ξ, ζ	Slopes of Gr_g and Gr_p in $\overline{Nu}_0$ and $\overline{Nu}$ correlations

Subscript

0	Static condition
lower	Lower edge of tilted open thermosyphon
upper	Upper edge of tilted open thermosyphon

Superscript

ZB	Zero buoyancy condition

Moreover, as the momentum flux inside the thermosyphon is diffused by viscous dissipations, the tube-wise flow momentum is getting weaker when the turbulent coolant flow penetrates toward the sealed end of each blind channel. The weakened momentum flux in the tube-wise direction causes different flow regimes in the orderthermosyphon [2]. This turbulence transition is attributed to the geometric confinements which damp out the turbulent activities in the tube-wise direction due to the shearing drags and the

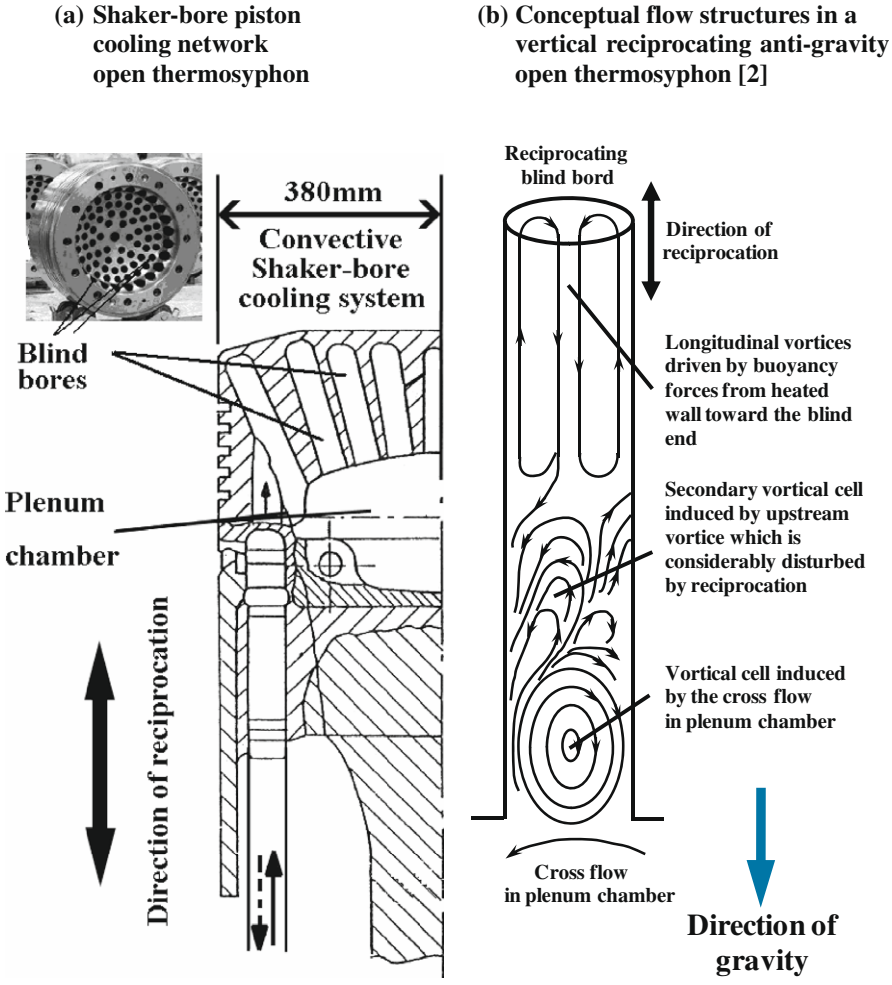

Fig. 1. (a) Multi-bore shaker cooling system in the piston of Sulzer RTA76 diesel engine series (b) conceptual flow structures in a heated vertical blind bore [2].

static pressures developed adjacent to the sealed end. Reflections of such turbulence transition taking place within the vortical cells on the heat transfer performances for an anti-gravity open thermosyphon are investigated here in order to resolve this industrial problem. This type of three-regime thermophysics in the open thermosyphon is basically retained in a likewise reciprocating channel but the vortical cells are subject to the temporal variations in a periodical manner [2]. Consequential heat transfer variations due to the flow modifications induced by reciprocation in the smooth and ribbed *vertical* open thermosyphons have been previously reported [1,2,4].

Based on the previous measurements of flow and heat transfer in the vertical reciprocating open thermosyphons [1,2,4], this research group starts probing into the thermophysics in a titled reciprocating open thermosyphon since the most of blind bores featured in Fig. 1a are tilted. Because the tube-wise directions of these tilted blind bores are no longer parallel to earth gravity and reciprocating forces, the vortical structures inside these tilted blind bores as well as the interacting manners between these vortices and the reciprocating force are modified from the scenarios developed in the vertical channel. A large number of previous studies examined the phenomena of heat convection in static open thermosyphons (cavities). These previous works have focused on investigating the effects on flow and heat transfer of different channel configurations, buoyancy levels, physical properties, channel aspect ratios and tilted angles as well as the manner in which the geometric and thermal boundary conditions in the thermosyphons (cavities) are considered [3,5–12]. Flow structures in an *open* cavity are also influenced by the flow pattern across its open surface and the geometrical features of the cavity and the plenum chamber [7]. In this regard, for a titled thermosyphon, a rich mode of vortical cells can be induced with their heat transfer performances modified from the vertical (0°) conditions [3]. There are two major streams, namely the upper stream going from the hot (bottom) to cold (top) ends and the lower stream going in the opposite direction inside the tilted tubular enclosure of AR = 9 [9,10]. Overall convective performances for tilted open thermosyphons depend greatly on the fluency of their exit heated flows.

With periodic buoyancy or reciprocating forces acting on the fluids inside cavities or thermosyphons [1,2], considerable modifications in fluid flow and heat transfer and/or the additional vortices from the static scenarios are reported by several research groups [1,2]. Introductions of periodic buoyancy forces via the pulsating heat fluxes from the heating surface [13] or by adding the vibrational buoyancy terms in the momentum equations [14–16] result in a variety of vortical flow structures in these cavities. The processes of vortex generation, convection and diffusion for these vibrating cavity flows are dynamic and vary with the oscillating frequency and amplitude of the vibrational forces. In this respect, increases of vibration frequency generally improve heat transfer but can also decrease heat transfer in the so-called intermediate vibrational convection regime [15,16]. Although the periodic forces acting on fluids in cavities can be introduced by the pulsating heat fluxes [13] or the additional vibrational forces [14–16], subtle differences in thermophysics still exist between the cavities examined in [14–16] and the reciprocating thermosyphons studied by [1,2,4,17]. In the case of reciprocating anti-gravity open thermosyphon, the channel is reciprocated that affect the buoyancy interaction and the flow condition developed over the open-end of the thermosyphon [1,2,4,17]. With weak reciprocating forces, heat transfer coefficients are initially impaired from the static levels but recovered after further increases of reciprocating forces in the vertical anti-gravity open thermosyphon with smooth or ribbed surfaces [1,4]. In the likewise reciprocating thermosyphon with twisted tape insert, the isolated reciprocating force effect consistently improves heat transfer at both sub-cooled and superheated conditions [17]. But none of the previously published works investigated the heat transfer in a simulated reciprocating *tilted* shaker-bored channel. Experiments were therefore performed for a reciprocating tilted thermosyphon. The direction of channel reciprocation is 15° away from the central axis of the open thermosyphon tube. By way of controlling the heat flux and the coolant flow rate into the system as well as the reciprocating frequency for a set of predefined geometrical and thermal boundary conditions, the test flow conditions are specified with their heat transfer distributions measured. Nevertheless, the zero mean flow velocity at each sectional plane of the thermosyphon prohibits the definition of Reynolds number (Re) based on the mean flow velocity. Instead, the characteristic flow velocity is conveniently calculated from the total mass flux fed into the plenum chamber with the characteristic length selected as the diameter of thermosyphon. The experimental details are described and followed by the illustrations of heat transfer results.

2. Experimental details

2.1. Dimensionless experimental parameters

The constructional details of the heat transfer test module along with the coordinate system adopted by present study are depicted in Fig. 2. The thermosyphon tube is circular in cross section with a tilting angle of 15° from the earth gravity. The open thermosyphon tube and the fluid plenum chamber reciprocate together with the coolant flowing into and out of the plenum chamber. While the geometric and thermal boundary conditions are predefined by the test section, the dimensionless parameters governing the thermophysics of this reciprocating thermosyphon can be identified from its flow equations. This set of flow equations has been derived by introducing a reciprocating frame of reference with the fluid motion described by this moving coordinate system [1].

For this study, the maximum variation in Pr for the test coolant (water) is 8.9% over the range of fluid temperatures tested. Therefore the impacts of Pr on Nu are not investigated here. This study is designed to permit the tube-wise wall temperature distributions along two opposite upper and lower edges of the thermosyphon tube to be examined over a range of flow and reciprocation conditions. For the geometrical and thermal boundary conditions specified by the heat transfer module as shown in Fig. 2, the measured heat transfer rates in terms of local Nu are related to Re, Pu, Gr_g or Gr_p [1] in the functional form of:

$$Nu = \Psi\{Re, Pu, Gr_g \text{ or } Gr_p\} \tag{1}$$

The interpolation and correlation of heat transfer results are based on Eq. (1) with the strategic aim to identify the heat transfer physics featured by Ψ function. The pulsating number (Pu) has its origin in the transient term of the total derivative of the momentum equation that expresses the ratio of the transient inertial forces induced by reciprocation to the fluid inertial forces. The gravitational and pulsating Grashof numbers Gr_g and Gr_p, respectively, express the relative buoyancy strength due to the earth gravity and reciprocating forces to viscous forces. The pulsating Grashof number (Gr_p) thus inherits the unsteadiness of the reciprocal nature and features the buoyancy interactions in the unsteady reciprocating flow field. It is worth noting that the gravity-induced free convection generally takes a period of time to stabilize the fluid temperature gradients among the flow field after which the Gr_g impacts on Nu are consequently realized. However, unless the period of reciprocation approaches infinite, the reciprocating flow is unlikely to offer the sufficient time for Gr_g effects to be developed but involved another type of buoyancy interactions for such an unsteady or the quasi-steady flow with their influences acting upon the vorticity of fluid.

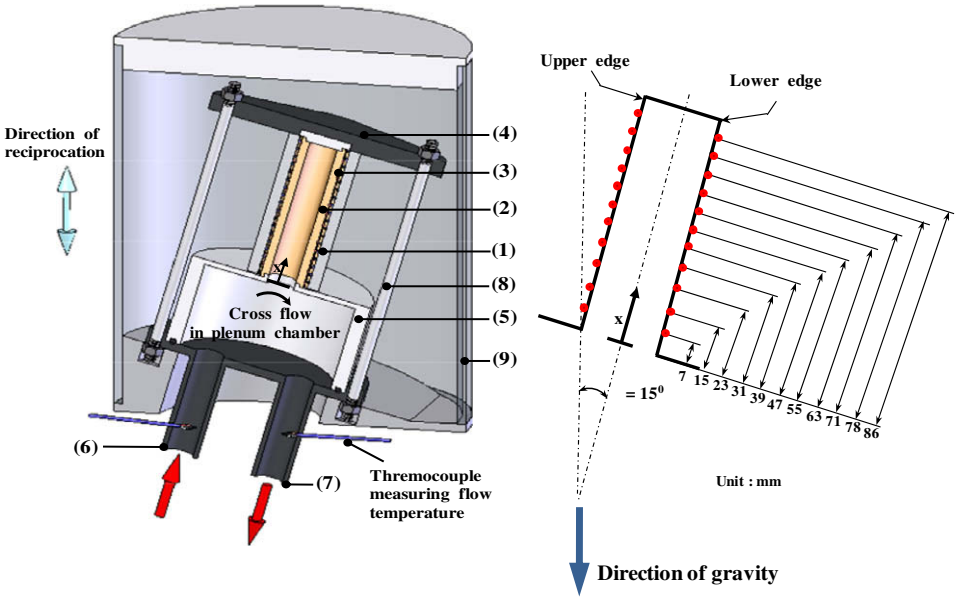

(1) Thermosyphon tube
(2) Thermocouple measuring wall temperature
(3) Electrical heating coil (4) Teflon top-wall (5) Plenum chamber
(6) Entrance tube (7) Exit tube (8) Draw bolt
(9) Stiffening tube

Fig. 2. Heat transfer test module.

Due to this physical consideration, Gr_g and Gr_p are separately selected to quantify the buoyancy levels in the static and reciprocating thermosyphon tubes. Eq. (2) expresses the local Nusselt number (Nu) defined experimentally.

$$Nu = q_f d/(T_w - T_f)k_f \quad (2)$$

In Eq. (2), the convective heat flux (q_f) is obtained by subtracting the external heat loss from the total heat flux for the tilted thermosyphon. The local heat loss flux is determined using the correlation derived from the results of a series of heat loss calibrations. At the highest heater power settings and reciprocating frequency tested, the maximum heat loss for heat transfer experiments is about 4.1% of the total heat flux. To comply with the common practices of studying heat transfer problems for cavity and thermosyphon flows [3,5–12], the reference fluid temperature (T_f) selected to define Nu in Eq. (2) is the fluid bulk temperature at the open entry plane of the thermosyphon tube. Local fluid properties such as specific heat, thermal conductivity and viscosity are determined by means of standard polynomial curve fitting functions based on the local film temperature of $(T_w + T_f)/2$. With the relevant fluid properties evaluated at the local film temperature, all the experimental raw data are processed into the dimensionless groups quoted in Eq. (1). The isolated and interactive impacts of the controlling parameters in Eq. (1) on Nu are examined with the relevant heat transfer correlations derived. Ranges of the governing dimensionless parameters for the tilted reciprocating open thermosyphon examined are listed in Table 1.

Table 1
Ranges of dimensionless parameters examined by this study

Reynolds number (Re)	5000–14,000
Pulsating number (Pu)	0–0.59
Gravitational Grashof number (Gr_g)	81,791–1,030,703
Pulsating Grashof number (Gr_p)	145,028–1,234,747

2.2. Experimental setup

The test rig that creates a reciprocating envelop within which a replaceable test module is fitted has been previously described [1]. The reciprocating motion of this test rig is created by the crank–wheel mechanism with adjustable frequencies in the range of 0–3 Hz that matches the piston running frequencies in a marine heavy-duty propulsive diesel engine. The stroke (S) of this reciprocating test rig is 300 mm. Fig. 2 shows the constructional details of the tilted circular open thermosyphon tube which is jointed with a cylindrical plenum chamber. The copper-made thermosyphon tube (1) is sealed at its top end and has the length (L) of 90 mm and inner diameter (d) of 15 mm with 2 mm wall-thickness giving the L/d ratio of 6. The stroke to tube-diameter ratio (S/d) of the present test assembly is 20 that agrees with the current geometrical specifications for such shaker-bore piston cooling configurations. Double screw threads with the same pitch of 4 mm but different depths of 1.5 and 1 mm are machined on the outer surface of the thermosyphon tube for the installation of thermocouples (2) and heater wires (3), respectively. Axial wall temperatures along two opposite upper and lower edges of the thermosyphon tube are detected by embedding Teflon insulated Ni–Ch/Ni–Al (K type) thermocouples with each sensing junction keeping 0.5 mm away from the inner surface of the tube (1). Eleven thermocouples with equal interval are attached axially along each of the two diametrically opposed edges with wall temperatures measured at the precise depth. Thermocouple junctions are secured by coating a layer of cement into the deeper groove to avoid the damages caused by reciprocating motion. The Ni/Ch alloy resistance heater wire is spirally wound into another shallow thread to create a basically uniform heat flux thermal boundary condition. Thermosyphon tube (1) is clamped between a 10 mm thick Teflon top-plate (4) and the Teflon-made cylindrical plenum chamber (5). The inner diameter and height of the plenum chamber are 100 and 50 mm, respectively. The coolant entrance (6) and exit (7) tubes of 12 mm in diameter permit the test coolant

(water) to flow in and out of the plenum chamber. The centers of the flow entrance and exit tubes (6)(7) are located 32.5 mm from the inner walls of plenum chamber (5). A stream of cross flow over the open-end of thermosyphon tube (1) is generated as shown in Fig. 2, which can induce a series of coherent vortices inside the blind thermosyphon tube. Therefore the geometries of thermosyphon tube, plenum chamber and the entry/exit piping configurations are inter-correlated to affect the heat transfer performances of the thermosyphon.

Two thermocouples penetrate into the central cores of the flow entry and exit tubes (6)(7) in order to measure the fluid temperatures into and out of the test module. The temperature rise of coolant through the heated test module (ΔT_f) is thus obtained as the temperature difference between the thermocouple measurements from the entry and exit tubes (6)(7). A routine check for ΔT_f is constantly performed during each heat transfer test using the enthalpy balance equation of $Q_f = \dot{m}Cp\Delta T_f$ in the attempt to ensure the energy balance of the heat transfer test module. Data batches can only be accepted when the discrepancies between the measured and calculated ΔT_f values are less than 10%. Four draw bolts (8) tighten the complete heat transfer test assembly, which was encapsulated within a stiffening Teflon tube (9) with the tilting angle (α) of 15° as shown in Fig. 2. The in fill of thermal insulation material packed in the space between the heated test section and the stiffening Teflon tube (9) minimizes the external heat loss. Table 2 summarizes the geometries of the test assembly.

This experimental study is a follow-up work of our previous study [17] which investigates the heat transfer in a likewise *vertically* static and reciprocating open thermosyphon at sub-cooled and superheated conditions. Heat transfer data collected from the present tilted anti-gravity open thermosyphon is compared with the data collected from the vertical thermosyphon [17] with the influences of the controlling parameters showed in Eq. (1) examined. The influences of Gr_g and Gr_p on Nu are revealed by comparing the heat transfer data generated with various buoyancy levels at fixed Re and Pu. This is achieved by adjusting the heater powers to control the wall temperatures near the top–end of the thermosyphon tube at a numbers of predefined values. All the temperature measurements are monitored and stored in a PC through a Net–Daq Fluke Hydra 2640A-100 data logger for the subsequent data processing.

2.3. Program

Local heat transfer measurements along the upper and lower edges of the tilted open thermosyphon at the static and reciprocating conditions are performed. In this way, the local Nu values along the static and reciprocating tilted thermosyphon at both sub-cooled (single phase) and superheated (two phase) conditions are generated and analyzed. This set of heat transfer data is produced at Re = 5000, 7500, 10,000, 12,500 and 14,000. At each selected Re, four sets of tests at the reciprocating frequencies of 0, 0.91, 1.25 and 1.67 Hz are performed. By way of comparing the heat transfer data obtained at static and reciprocating conditions, the effects of reciprocation on heat transfer inside the tilted open thermosyphon are revealed. At each Re/Pu combination, thirteen different levels of heater power are supplied to raise the wall temperatures at the sealed end of the thermosyphon tube to the nominal values of 313, 323, 333, 343, 353, 363, 373, 383, 393, 403, 413, 423 and 433 K. The range of heat flux measurements is 780-17500 Wm^{-2}. Data batches obtained with different Gr_g or Gr_p values at fixed Re and Pu reveal the buoyancy impacts on heat transfer. All the heat transfer data collected from the thermosyphon tube are analyzed parametrically with the attempt to generate a set of empirical heat transfer correlations that permits all the relevant physical effects governing the system's behavior to be examined.

Table 2
Geometric features of heat transfer test section

Geometric dimensionless groups	Dimensionless ratio
Height-to-diameter ratio of thermosyphon tube = 90 mm/15 mm	6
Height-to-diameter ratio of plenum chamber = 50 mm/100 mm	0.5
Stroke-to-diameter ratio of thermosyphon tube = 300 mm/15 mm	20
Tilting angle of thermosyphon tube	15°

The fluid properties such as the viscosity and density of the coolant are subject to variances when the fluid temperatures are varied during heat transfer tests. The mass flow rate fed into this flow system is constantly adjusted to limit such variations in Re and Pu at the entrance of the plenum chamber to within ±1% of the targeting values. The instantaneous temperature measurements for every period of 10 seconds are detected, stored and averaged to provide the time-averaged temperature measurements. The instantaneous and time-averaged temperature measurements are constantly scanned on the screen of PC. This study assumes the flow reaches the quasi-steady state when the variations of the time-averaged wall temperatures remain within ±0.3 °C for several successive scans for a specified measurement spot. A period of about 50 min is generally required to achieve such quasi-steady state. Having satisfied the conditions of energy balance and the quasi-steady state assumption, all the relevant raw measurements are stored as a data batch and converted into the dimensionless groups listed in Eq. (1). The experimental uncertainties for the dimensionless parameters generated here is performed [18]. By treating the maximum uncertainty in temperature measurement of ±0.3 °C as the optimistic condition with the temperature difference between wall and fluid reference condition varied from 25 to 145 K, the maximum uncertainty in Nu, Re, Pu, Gr_g and Gr_p are 8.9, 7.6, 6.3, 8.8 and 9.8%, respectively.

3. Results and discussion

3.1. Static tilted anti-gravity open thermosyphon

The present static and reciprocating anti-gravity open thermosyphon has a tilting angle of 15° from the gravitational and reciprocating forces. In the absence of reciprocation for the present flow configuration, Nu_0 is dependent on Re and Gr_g alone. Fig. 3 typifies (a) boiling curve at X/d = 4.7 and (b) wall temperature (T_w) and (c) Nu_0 distributions along the upper and lower edges of the static thermosyphon tube at Re = 5000 and 10,000 in which the Nu_0 data collected from the likewise anti-gravity open thermosyphon with 0° inclination (vertical condition) is compared [17]. As shown in Fig. 3a, the transition of single phase convection, constituting the regime of partial nucleate boiling, is observed at each Re tested. For this tilted thermosyphon, increases of Gr_g lead to heat transfer improvements so that $\partial q_f/\partial(T_w - T_{sat})$ increases accordingly as $T_w - T_{sat}$ increases. After transiting the partial boiling regime as shown in Fig. 3a, the values of $\partial q_f/\partial(T_w - T_{sat})$ are further increased; featuring the fully developed nucleate boiling regime. The T_w values that initiate the developed nucleate boiling are approximated at 125 °C for this tilted thermosyphon. The typical tube-wise T_w variations in the developed nucleate boiling regime are shown in Fig. 3b. Wall temperatures drop at the entry and seal ends of the tilted thermosyphon; which has led to the regional heat transfer elevations. Fig. 3b shows no appreciable T_w differences between the upper and lower edges; except at the immediate flow entrances where the regional bifilamental entry and exit streams are likely developed. This incurs the slight higher Nu_0 at the lower edge than its upper counterpart at the immediate

entrance as seen in Fig. 3c. Except at the immediate entry locations, there is no appreciable heat transfer difference between the upper and lower edges found in Fig. 3c for both tilted and vertical *anti-gravity* open thermosyphon tubes at the static condition due to the influence of anti-gravity mechanism which prohibits the formation of bifilamental flows over the entire tilted static tube. However, it has been previously demonstrated [17] that the negligible upper-to-lower Nu_0 differences for the vertical anti-gravity open thermosyphon at both static and reciprocating conditions [2] are the results of the vortical structures as seen in Fig. 1b. Therefore the Nu_0 results depicted by Fig. 3c infers the development of vortical flow cells in present tilted blind tube rather than the bifilamental flows in the tilted blind tube which is not operated at the anti-gravity condition [9,10,19,20]. Data bands of Nu_0 at each measurement station driven by the cited ranges of Gr_g as shown in Fig. 3c reflect the degrees of gravitational buoyancy impacts on heat transfer. The upward Nu_0 data-band as shown for the present tilted static open thermosyphon reveals the improving effect of gravitational buoyancy on local heat transfer. The heat transfer performances in the tilted open thermosyphon are considerably improved from the scenarios in the vertical thermosyphon. The much improved heat transfer performances with enlarged Gr_g impacts on Nu_0 in present tilted thermosyphon from the vertical references as compared in Fig. 3c suggest that the vortical circulations in the tilted anti-gravity open thermosyphon are more rigorous from the vertical tube conditions.

A parametric study of the gravitational buoyancy impact on heat transfer is performed by plotting Nu_0 against the buoyancy parameter with the asymptotic Nu_0 values at the conditions of vanished wall-to-fluid temperature differences ($Gr_g \to 0$) identified. This procedure reveals the heat transfer levels at the tested *Re* without buoyancy interaction. An additional set of heat transfer data corresponding to the so called zero-buoyancy conditions in terms of Nu_0^{ZB} is generated and the individual *Re* impacts on Nu_0^{ZB} are accordingly examined. The impacts of gravitational buoyancy on Nu_0 as well as the asymptotic Nu_0^{ZB} values are revealed by plotting Nu_0 against the gravitational buoyancy parameter in terms of Gr_g/Re^2 at different axial locations as shown in Fig. 4. Also compared in each plot of Fig. 4 are the heat transfer results collected at the same axial spot from the vertical static anti-gravity open

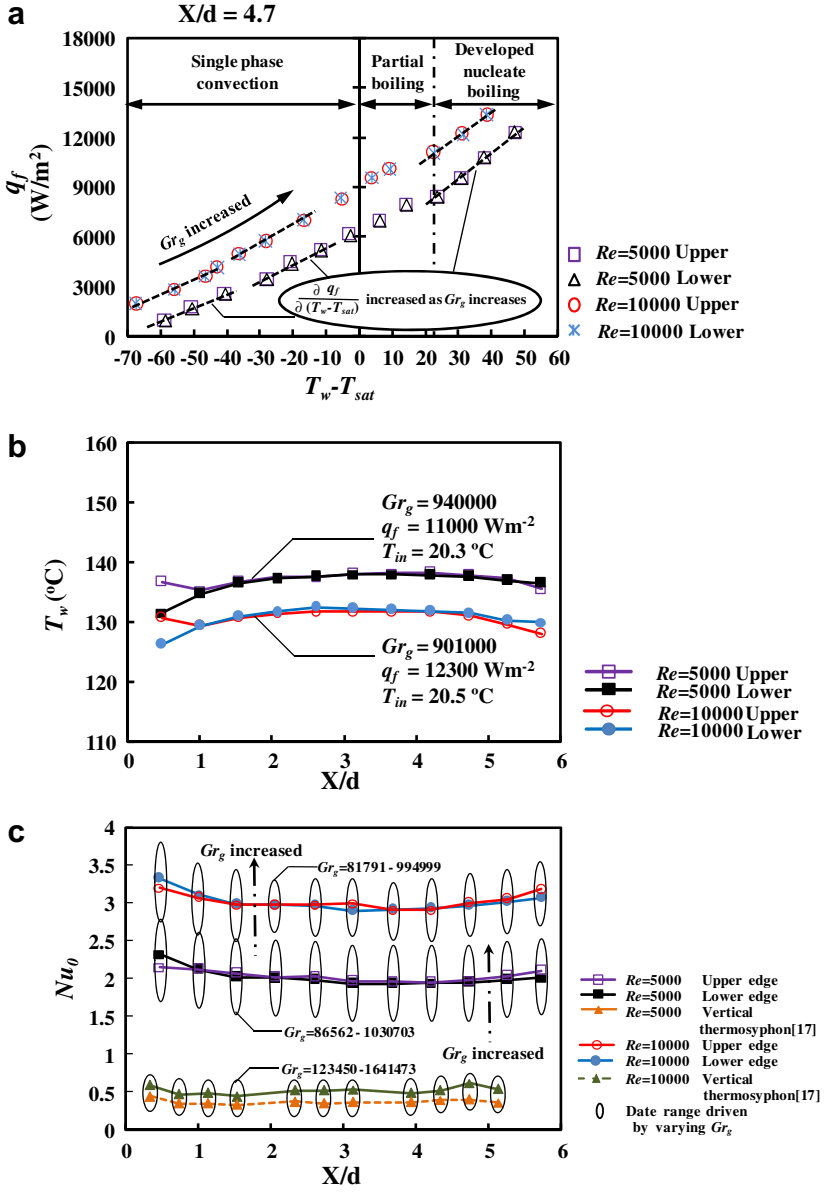

Fig. 3. (a) Boiling curve (b) T_w (c) Nu_0 distributions along upper and lower edges of tilted and vertical static blind tube at *Re* = 5000 and 10,000.

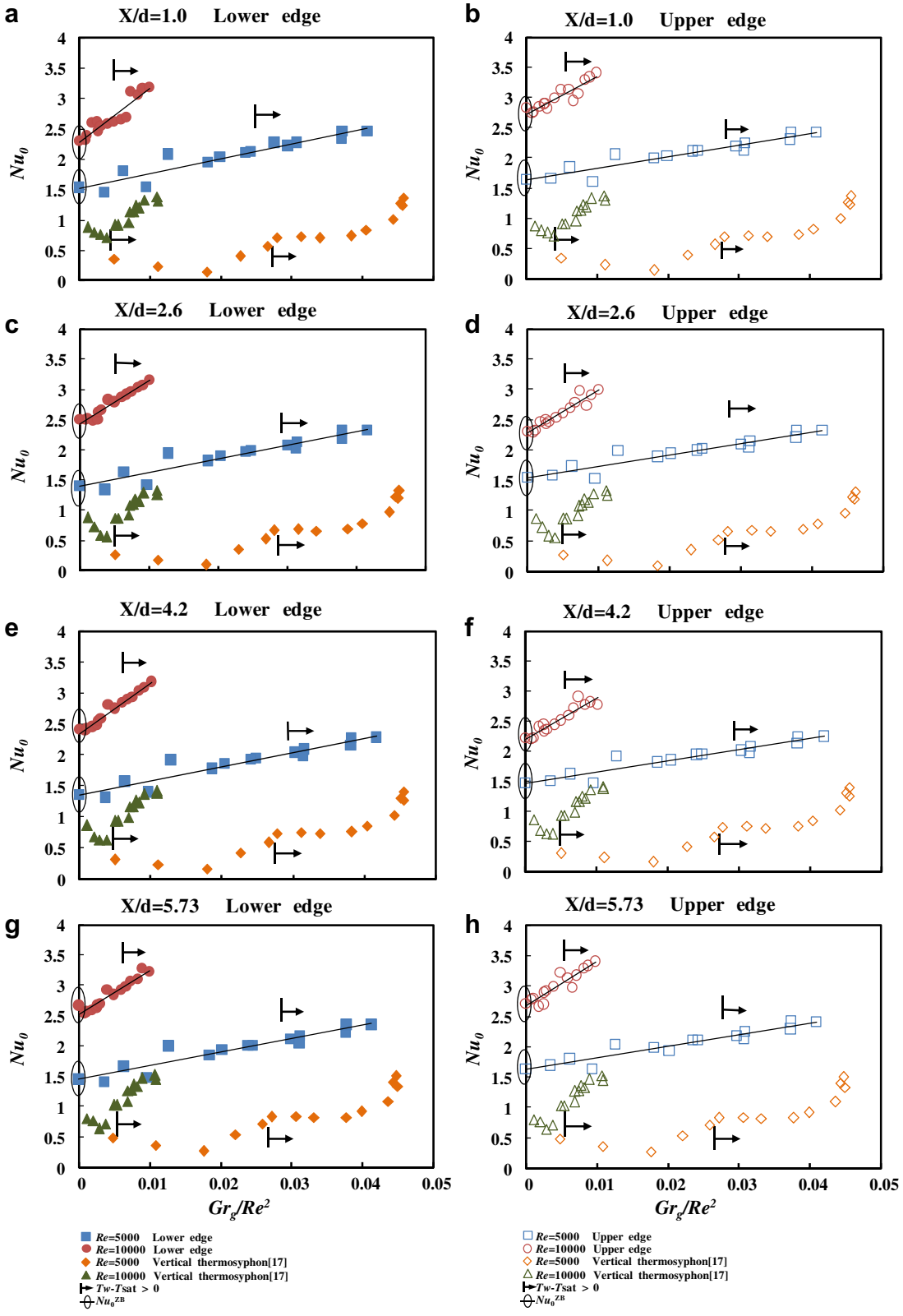

Fig. 4. Variations of Nu_0 with Gr_g/Re^2 along (a)(c)(e)(g) upper and (b)(d)(f)(h) lower edges of static blind tube with Re = 5000 and 10,000 at various X/d locations.

thermosyphon [17]. In each plot of Fig. 4, a symbol marked in each Gr_g/Re^2 controlled data trend at the selected Re separates the flow regimes into the sub-cooled ($T_w - T_{sat} < 0$) and superheated ($T_w - T_{sat} > 0$) conditions. In the tilted anti-gravity open thermosyphon as shown in Fig. 4, the heat transfer coefficients consistently increase as Gr_g/Re^2 increases. Gravitational buoyancy impacts in such a tilted anti-gravity open thermosyphon improve local heat transfer. Recalling the previous statement that infers the existence of vortical cells in such a deep tilted anti-gravity open thermosyphon, the favorable buoyancy impacts for heat transfer perfor-

mances at both sub-cooled and superheated regimes are likely related to the improved penetration of cold stream into the tilted thermosyphon as Gr_g/Re^2 increases. The cross examination of heat transfer results collected from the upper and lower edges of the vertical and tilted anti-gravity open thermosyphon tubes as shown in Fig. 4 reconfirms the negligible upper-to-lower heat transfer differences as described previously. The Nu_0^{ZB} level at the limiting condition of $Gr_g/Re^2 = 0$ for each Re tested is marked on the vertical axis of each plot shown in Fig. 4. The correlation procedure is demonstrated by fitting the linear line through each Re controlled data series that numerically extrapolates back to the origin of $Gr_g/Re^2 = 0$. It is noticed that the averaged Nusselt number ($\overline{Nu_0}$) evaluated from all the Nu_0 data detected along the upper and lower edges of the tilted static blind tube also inherits the heat transfer characteristics depicted in Fig. 4. Justified by all the curve-fitting versions of Nu_0 and $\overline{Nu_0}$ versus Gr_g/Re^2 as typified in Fig. 4 for the present tilted anti-gravity open thermosyphon, the local (Nu_0) and averaged ($\overline{Nu_0}$) heat transfer levels are correlated as:

$$Nu_0(\overline{Nu_0}) = Nu_0^{ZB}(\overline{Nu_0^{ZB}})\{Re\} + \xi\{Re\} \times Gr_g/Re^2 \quad (3)$$

The slope of each fitted line (ξ) in Eq. (3) varies with Re so that the heat transfer coefficient for this tilted static anti-gravity open thermosyphon is inter-correlated with Re and Gr_g/Re^2. As the convective heat transfer capacities in such a tilted *static* blind tube are generated by the external cross stream over the open entrance that induces coherent vortical flow-cells in the thermosyphon tube, the increasing strength of the cross stream over the open entrance due to the increase of Re strengthens the in-tube vortical circulations. Therefore the Nu_0^{ZB} value increases as Re increases. This is clearly shown in Fig. 5a where the Nu_0^{ZB} value increases linearly with the increase of Re. Fig. 5b shows the increased ξ slope as Re increases. Therefore the increase of Re amplifies the buoyancy impacts in the tilted static open thermosyphon. Combining the data trends typified in Fig. 5a and b gives the heat transfer correlations for Nu_0 and $\overline{Nu_0}$. The set of Nu_0 correlation is treated as the heat transfer reference to normalize the heat transfer data collected from the reciprocating test tube in order to highlight the impacts of reciprocation on local heat transfer. The correlation derived for $\overline{Nu_0}$ expressed in Eq. (4) is generated for design applications.

$$\overline{Nu_0} = (2.55E-4 \times Re + 0.0937) + (74.66 - 0.022 \times Re + 2E - 7 \times Re^2) \times Gr_g/Re^2 \quad (4)$$

3.2. Reciprocating tilted anti-gravity open thermosyphon

The reciprocating force acting on fluids as the volumetric body force in the present tilted anti-gravity open thermosyphon varies periodically and is functionally related with the density distribution of fluids. Thus the temporally varied reciprocating force inevitably involves buoyancy interactions due to relative temperature differences among the flow. Such quasi-steady flow system produces the attendant temporal heat transfer variations. The heat transfer data presented here is the temporally averaged value from the time-wise heat transfer measurements for a period of 10 sec. Fig. 6 compares the tube-wise Nu distributions between the tilted and vertical open thermosyphon tubes at $Re = 7500$ and 10,000 with two reciprocating frequencies of 1.25 and 1.67 Hz. The tube-wise Nu distributions as shown in Fig. 6a and b at various pulsating and Reynolds numbers are clearly different from the axial Nu_0 variations showed in Fig. 3. The flow structures in this tilted reciprocating anti-gravity open thermosyphon undergo a transition process from the vortical cells to the bifilamental stratified streams as Pu increases systematically. In the static tilted blind tube, there is negligible heat transfer difference between the upper and lower edges. But the heat transfer differences between the upper and lower edges for this tilted reciprocating blind tube with the higher Nu levels along the upper edge proceed over the axial region of $0 < X/d < 3$ as seen in Fig. 6a for both sets of tested Re and Pu. Moving toward the sealed end of the tilted blind tube over the second half region of $3 < X/d < 6$ as seen in Fig. 6a, there is no appreciable upper-to-lower Nu difference. The different Nu levels between the upper and lower edges in the axial region of $0 < X/d < 3$ reflect the development of bifilamental flows. At these particular sets of reciprocating conditions featured by Fig. 6a, a pair of cold (entry) and hot (exit) stratified streams convects through the open entrance of this tilted reciprocating blind tube along its upper and lower edges, respectively. Beyond the axial region of $0 < X/d < 3$, the flow structures gradually yield into the vortical cells so that the upper-to-lower Nu differences are vanished in the second half region of $3 < X/d < 6$. Further increase of Pu to the conditions specified by Fig. 6b at each selected Re, the bifilamental flow structures prevail over the entire length of this tilted reciprocating blind tube, leading to the appreciable upper-to-lower Nu differences throughout the reciprocating tube as seen in Fig. 6b. It is noticed that the increase of reciprocating frequency from 1.25 Hz (Fig. 6a) to 1.67 Hz (Fig. 6b) produces the corresponding increases in Pu from 0.31 to 0.38 at $Re = 7500$ and from 0.23 to 0.28 at $Re = 10{,}000$. The critical pulsating numbers for such flow transition from vortical cells to bifilamental flows are Re dependent. Particularly, the upper-to-lower Nu differences switch-over to the scenarios with the higher heat transfer rates along the lower edge in the second half region of $3 < X/d < 6$ as seen in Fig. 6b. The pair of stratified cold and hot streams within the entire tilted reciprocating blind tube is twisted at the axial location about the half length ($L/2$) of the blind tube after further enhancing the relative

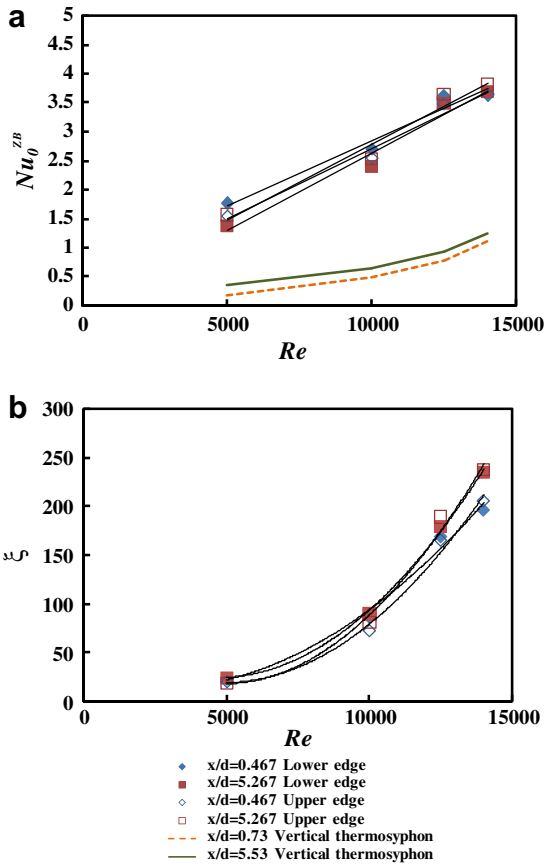

Fig. 5. Variations of (a) Nu_0^{ZB} and (b) ξ value with Re.

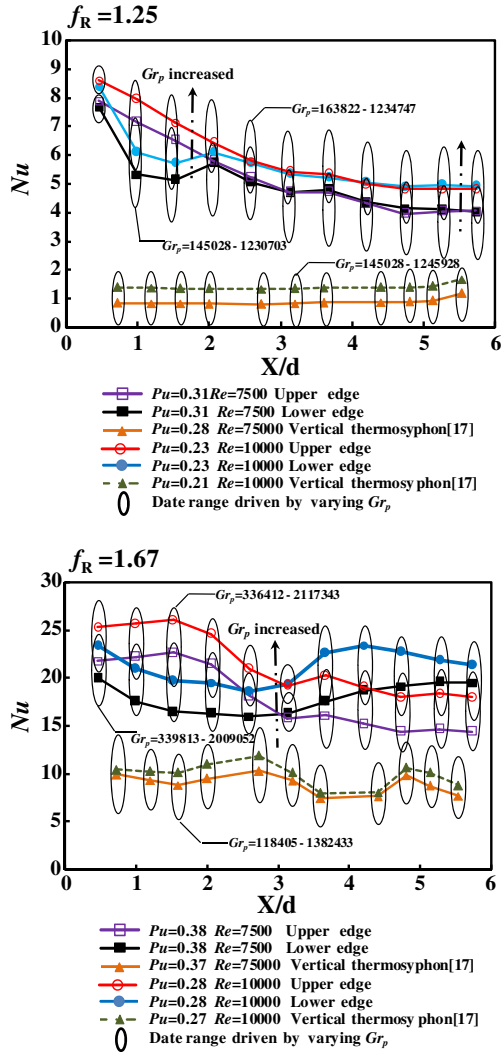

Fig. 6. *X*-wise *Nu* distributions along upper and lower edges of tilted and vertical reciprocating anti-gravity open thermosyphon tubes.

strengths of reciprocating forces to the conditions featured by Fig. 6b. Such flow transition from the vortical cells to the bifilamental stratified streams as *Pu* increases is triggered by the reciprocation forces acting on the *tilted* anti-gravity open thermosyphon. However, there is no such flow transition observed for a likewise *vertical* reciprocating blind tube [17].

The *Nu* levels collected from the tilted reciprocating anti-gravity open thermosyphon tube as shown in Fig. 6a and b are consistently higher than the counterparts of vertical blind tube. The channel inclination once again improves the fluency of fluid flow in the reciprocating anti-gravity open thermosyphon via the process of flow transition from the vortical cells to the bifilamental streams. For both the vertical and tilted reciprocating blind tubes at sub-cooled and superheated conditions, local *Nu* values consistently increase as Gr_p increases. Buoyancy interactions in the vertical and tilted reciprocating anti-gravity open thermosyphon tubes improve heat transfer. In general, the ranges of *Nu* bands driven by varying Gr_p along the tilted reciprocating tube are larger than those along the vertical tube as seen in Fig. 6a and b. This confirms the higher degrees of buoyancy impact on heat transfer in the tilted reciprocating tube. But at the switch-over location near 3X/*d* as shown in Fig. 6b, the *Nu* range driven by varying Gr_p is considerably suppressed at these reciprocating conditions. The local buoyancy impacts at the location where the bifilamental streams start twisting become less effective. Justified by the various tube-wise *Nu* profiles obtained with different *Re* and *Pu* as shown in Fig. 6, the upper-to-lower heat transfer difference due to the transition of flow structures in this tilted reciprocating blind tube appears to be *Re* and *Pu* dependent.

Fig. 7 reveals the tube-wise variations of the upper-to-lower *Nu* difference as *Pu* increases at two selected Reynolds numbers of 7500 and 10,000. Each plot of Fig. 7 which depicts four different sets of tube-wise Nu_{Upper}/Nu_{Lower} ratios at four reciprocating frequencies of 0, 0.92, 1.25 and 1.67 Hz clearly indicates the manner by which the upper-to-lower *Nu* differences gradually develop from the open entrance toward the sealed end as *Pu* increases. While the evident *Nu* differences between the upper and lower edges along the tilted blind tube over the region of $0 < X/d < 3$ are observed at the reciprocating frequency (f_R) of 0.92 Hz as shown in Fig. 7a and b, the upper-to-lower *Nu* difference over the region of $3 < X/d < 6$ has not yet developed. A further increase of reciprocating frequency from 0.92 to 1.25 Hz at *Re* = 7500 or 10,000,which leads to the increase of *Pu*, has amplified the Nu_{Upper}/Nu_{Lower} ratios over the region of $0 < X/d < 3$ and initiated the upper-to-lower *Nu* differences over the region of $3 < X/d < 6$. Although the ratios of Nu_{Upper}/Nu_{Lower} are generally increased as *Pu* increases, the degrees of upper-to-lower *Nu* differences over the region of $0 < X/d < 3$ are considerably higher than those in the region of $3 < X/d < 6$. It is worth noting that the wavy-like Nu_{Upper}/Nu_{Lower} profiles along the tilted reciprocating tube as typified in Fig. 7a and b are generated by the wall temperature (T_w) distributions along two diametrically opposite upper and lower edges under the condition of the uniform heating flux. In view of these two sets of wavy Nu_{Upper}/Nu_{Lower} or T_w profiles as shown in Fig. 7a and b, the bifilamental hot and cold stratified streams in this tilted reciprocating blind tube seem to be gradually emerged with the tendency of evolving into a pair of three dimensional spiral structures as *Pu* increases systematically. In this respect, the detailed flow measure-

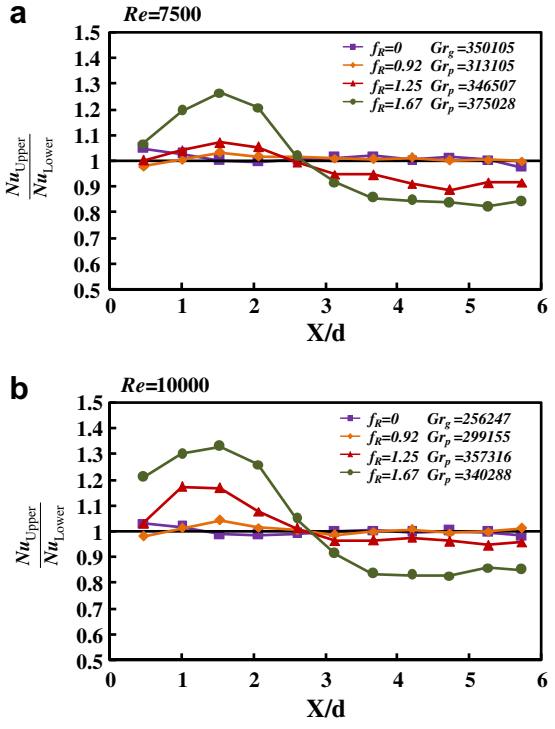

Fig. 7. *X*-wise distributions of Nu_{Upper}/Nu_{Lower} ratio at *Re* = (a) 7500 and (b) 10,000 with reciprocating frequencies of 0, 0.92, 1.25 and 1.67 Hz.

ments are necessary in order to clear the flow physics responsible to the heat transfer performances observed in Fig. 7.

Following the procedure of analyzing the buoyancy effect that constructs Fig. 4, as well as the initial step to derive the heat transfer correlation for this tilted reciprocating blind tube, the *Nu* values detected along the upper and lower edges at the axial location of 1.53 *X*/*d* with various *Re* and *Pu* for the fixed reciprocating frequency (f_R) of 1.67 Hz are plotted against Gr_p/Re^2 as shown in Fig. 8. With a fixed f_R value, the increase of *Re* reduces *Pu*. As typified in Fig. 8 for any set of *Re* and *Pu* tested, each *Nu* data series increases linearly as Gr_p/Re^2 increases for both sub-cooled and superheated regimes. The slope for such Gr_p/Re^2 controlled data trend as shown in Fig. 8 increases with the increase of *Re*. The physical implication for such increased slope driven by increasing *Re* is the enhanced buoyancy effect as the inertial force effect enhances. Clearly there is inter-correlation between *Re* and Gr_p/Re^2 in the *Nu* correlation. But, instead of the improved coolant penetration due to the enhanced strengths of vortices developed in the tilted *static* blind tube by increasing Gr_g/Re^2, the elevation of buoyancy level in the tilted *reciprocating* blind tube tends to accelerate the bifilamental hot and cold stratified streams and leads to the heat transfer improvement. Relative to the vertical reciprocating blind tube [17] as compared in Fig. 8, the tilted blind tube still offers the higher heat transfer levels under the reciprocating conditions. The extrapolation of each data trend as indicated in Fig. 8 toward the limiting condition of $Gr_p/Re^2 = 0$ reveals the zero-buoyancy *Nu* level (Nu^{ZB}) corresponding to the prescribed *Re* and *Pu*. As shown by the remarks on the vertical axis of Fig. 8, the Nu^{ZB} values are *Re* and *Pu* dependent.

The variation of Nu^{ZB} againt *Pu* for each tested *Re* of 5000, 10,000, 12,500 or 14000 at 1.53 *X*/*d* along the upper and lower edges of the tilted reciprocating blind tube is shown in Fig. 9. At the limiting conditions of $Gr_p = 0$ and *Pu* = 0, the heat transfer solutions recast the Nu_0^{ZB} values obtained with the same *Re*. At each *Re* tested, the Nu^{ZB} values are initially reduced from the static Nu_0^{ZB} level as *Pu* increases. Such heat transfer impediments acting by the *Pu* effect alone with relatively weak reciprocating forces has been attributed to the undermined coolant penetration into the reciprocating anti-gravity open thermosyphon [2,21]. But with the further increase of *Pu*, heat transfer levels for this tilted reciprocating blind tube are soon recovered and enhanced to the levels well above than the static references. This particular Nu^{ZB} versus *Pu* pattern is followed by all the results with different *Re* tested and agrees with the results reported in [17] for the likewise vertical reciprocating blind tube. The pulsating numbers above which the Nu^{ZB} values turn above than Nu_0^{ZB} references systematically decrease as *Re* increases. Therefore the f_R range within which the weak reciprocation undermines the heat transfer performance in this tilted blind tube is constricted as *Re* increases. The individual *Pu* effect on heat transfer without buoyancy interaction at each tested *Re* is featured by each curve indicated in Fig. 9. As such *Pu*

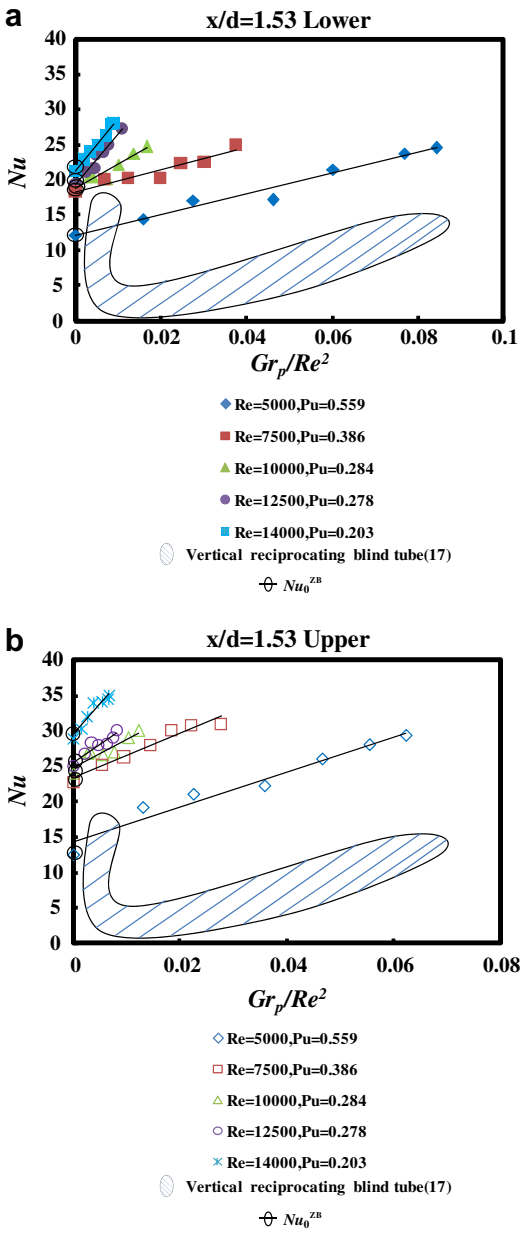

Fig. 8. Variations of *Nu* with Gr_p/Re^2 along (a) upper (b) lower edges of reciprocating blind tube at f_R = 1.67 Hz with various *Re* and *Pu* at 1.53 *X*/*d*.

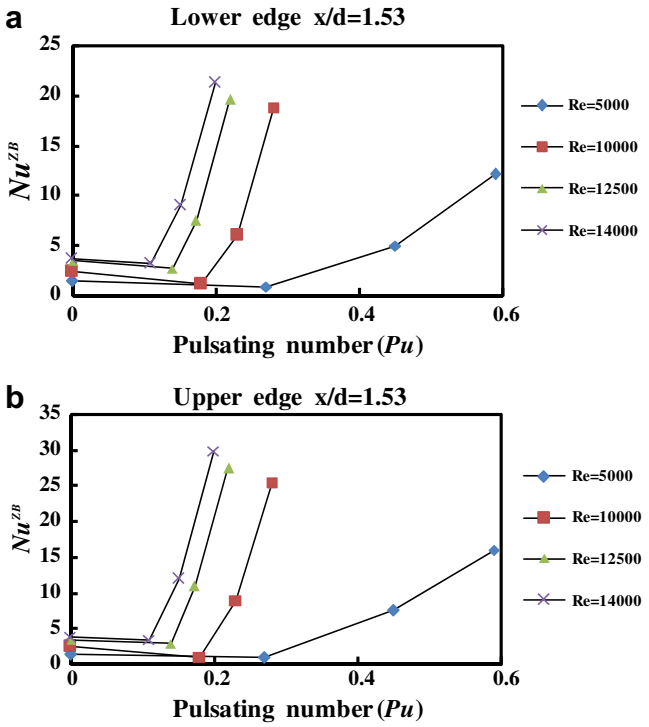

Fig. 9. Nu^{ZB} versus *Pu* with *Re* = 5000, 10,000, 12,500 and 14,000 at 1.53 *X*/*d* along the upper and lower edges of the tilted reciprocating blind tube.

controlled Nu^{ZB} variations are segregated by Re, the inter-correlative Re-Pu effect on Nu^{ZB} is evident.

3.3. Heat transfer correlation

Having clarified the heat transfer physics for the present tilted reciprocating anti-gravity open thermosyphon, the Nu correlation is constructed using Re, Pu and Gr_p as the controlling parameters. To take these parametric effects into account, the Nu correlation is derived based on the data trend revealed in Fig. 8. This correlating procedure is shown by adding the fitted line through each Re and Pu controlled data series back to the origin of $Gr_p/Re^2 = 0$. However, instead of deriving the heat transfer correlations for local Nu values, all the Nusselt numbers collected from the tilted blind tube at each reciprocating test condition are averaged as $\overline{Nu}$ with its correlation derived here in order to enhance the generality for piston cooling applications. The averaged $\overline{Nu}$ values also follow the data trends depicted in Fig. 8 which are accordingly correlated as:

$$\overline{Nu} = \overline{Nu}^{ZB}\{Re, Pu\} + \zeta\{Re, Pu\} \times Gr_p/Re^2 \quad (5)$$

with the reciprocating force effects involved, the zero-buoyancy heat transfer level ($\overline{Nu}^{ZB}$) and the degree of buoyancy impact indexed by ζ value in Eq. (5) are functions of Re and Pu. The mathematic structure defined in Eq. (5) allows the inter-correlative relationships between Re, Pu and Gr_g/Re^2 to be developed. While the variations of $\overline{Nu}^{ZB}$ against Pu follow the typical data trends shown by Fig. 9, the varying manners of $\overline{Nu}^{ZB}$ and ζ value against Pu are summarized in Fig. 10a and b, respectively. As described previously, the values of $\overline{Nu}^{ZB}$ and ζ at the static condition with $Pu = 0$ are, respectively, forced to be the $\overline{Nu}_0^{ZB}$ value and the slope of each Re controlled data trend in the $\overline{Nu}_0$ versus Gr_g plot. Data trends showed by Fig. 10a follow the patterns revealed in Fig. 9. As shown in Fig. 10b, all the ζ values remain positive to reflect the improved heat transfer performance by increasing the reciprocating buoyancy level. But the ζ values increase with the increase of Re or Pu. Therefore both synergetic Re and Pu effects amplify the improving buoyancy effects on heat transfer in the present tilted reciprocating anti-gravity open thermosyphon. Led by all Re versions of Fig. 10a and b, it is proposed that the functions of $\overline{Nu}^{ZB}$ and ζ can be well fitted by two quadratic functions of:

$$\overline{Nu}^{ZB} = a_0\{Re\} + a_1\{Re\} \times Pu + a_2\{Re\} \times Pu^2 \quad (6)$$

$$\zeta = b_0\{Re\} + b_1\{Re\} \times Pu + b_2\{Re\} \times Pu^2 \quad (7)$$

where a_s and b_s are functions of Re. The variations of a_s and b_s coefficients are plotted against Re to disclose the functional structures of a_s and b_s coefficients with Re as the controlling variable. In the a_0 versus Re plot, it is noticed that a_0 value approaches zero as $Re \to 0$. Therefore the tilted reciprocating blind tube without any buoyancy involved at the zero flow condition has vanished forced convective capability. Justified by the various data trends revealed in these a_s versus Re and b_s versus Re plots, the numerically determined curve fits for a_s and b_s coefficients are derived and listed in Table 3.

Table 3
Correlative a_s and b_s functions

Coefficient	Correlative equation
a_0	$a_0 = 3.03E\text{-}4 \times Re$
a_1	$a_1 = -43.42 + 0.009 \times Re - 6E\text{-}07 \times Re^2$
a_2	$a_2 = 209.4 - 0.065 \times Re + 7E\text{-}06 \times Re^2$
b_0	$b_0 = 101.9 - 0.032 \times Re + 3E\text{-}06 \times Re^2$
b_1	$b_1 = -655.1 + 0.179 \times Re - 1E\text{-}05 \times Re^2$
b_2	$b_2 = 2.29E4 - 6.73 \times Re + 4.65E\text{-}4 \times Re^2$

A set of heat transfer correlations evaluating $\overline{Nu}$ value for the tilted reciprocating anti-gravity open thermosyphon has been derived as Eqs. (5)–(7). The two sets of equations for $\overline{Nu}_0$ and $\overline{Nu}$ are representative for all the experimental heat transfer data generated by the present study and resolve the synergetic influences of inertial, reciprocating and buoyancy forces on heat transfer. All

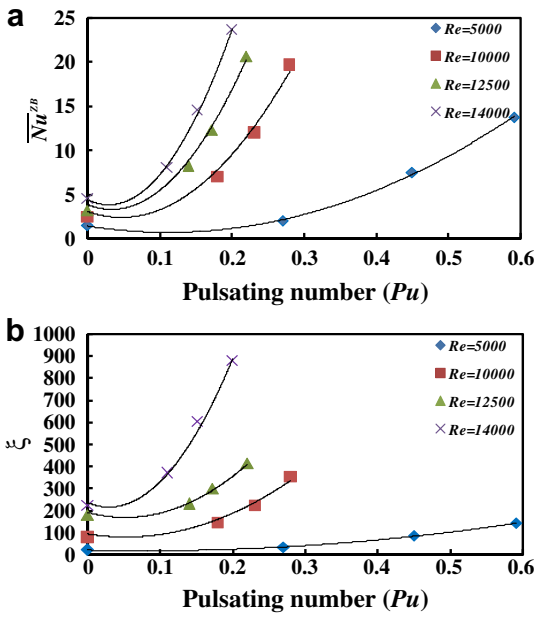

Fig. 10. Variations of (a) $\overline{Nu}^{ZB}$ and (b) ζ value against Pu at $Re = 5000$, 10,000, 12,500, 14,000.

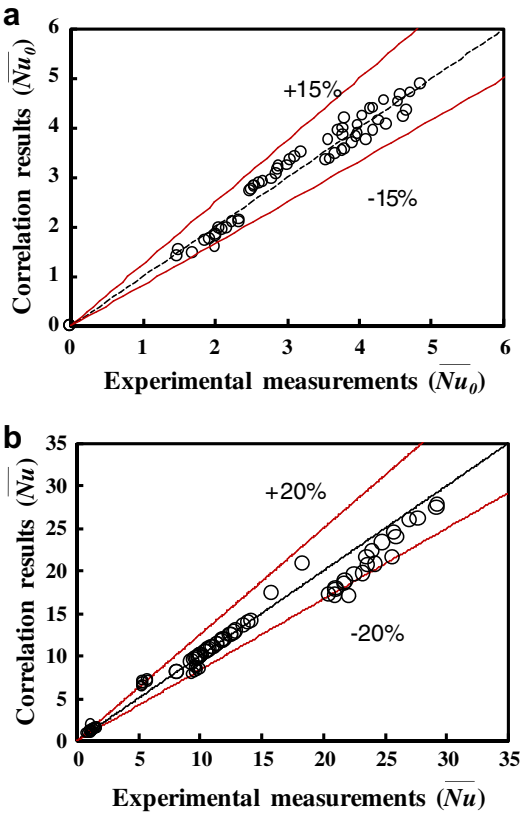

Fig. 11. Comparisons of experimental measurements and correlation results for (a) $\overline{Nu}_0$ and (b) $\overline{Nu}$.

the experimental data and the correlative predictions using Eq. (4) for $\overline{Nu}_0$ and Eqs. (5)–(7) for $\overline{Nu}$ are compared to examine the overall success of these correlations. As indicated in Figs. 11a and 12b, 95 and 90% of the present $\overline{Nu}_0$ and $\overline{Nu}$ data are found to agree within ±15 and 20% of the correlations proposed over the entire parametric ranges tested. Consider the precisions achieved by Eq. (4) for $\overline{Nu}_0$ and Eqs. (5)–(7) for $\overline{Nu}$, these proposed correlations could offer a good indication for the overall heat transfer capabilities of this tilted static and reciprocating blind tubes.

With the assist of the derived $\overline{Nu}_0$ and $\overline{Nu}$ correlations, the charts which refers to the reciprocation induced relative heat transfer modifications from the static references as the $\overline{Nu}/\overline{Nu}_0$

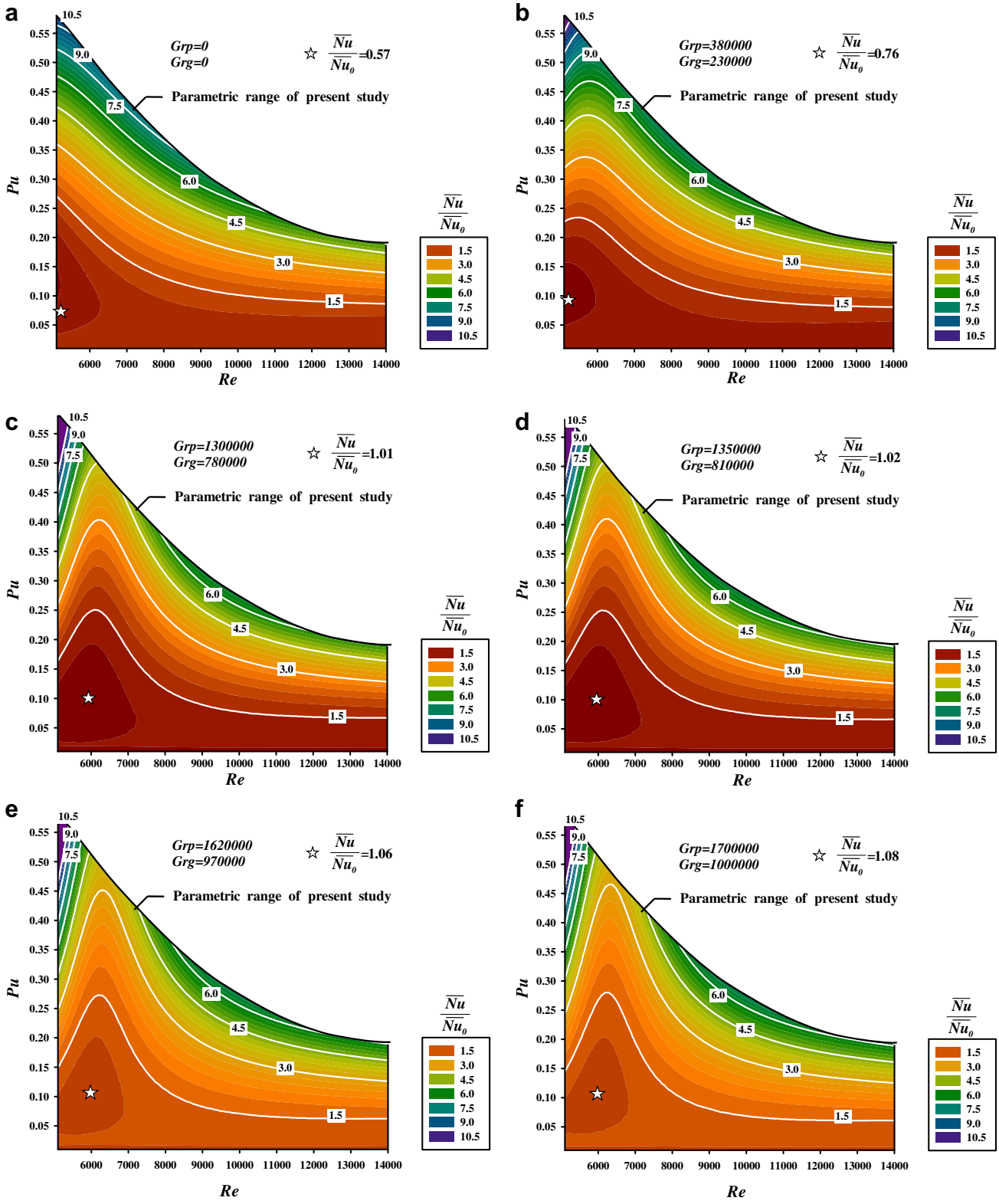

Fig. 12. *Re* and *Pu* controlled $\overline{Nu}/\overline{Nu}_0$ contours with various buoyancy levels.

ratios are constructed for this tilted anti-gravity open thermosyphon. It is noticed that the $\overline{Nu}_0$ level is determined using Eq. (5) with the Gr_g value evaluated from the wall-to-fluid temperature difference recorded for the reciprocating flow condition that generates $\overline{Nu}$ value. Within the parametric conditions covered by the present study, Fig. 12 depicts the variations of $\overline{Nu}/\overline{Nu}_0$ contours against *Re* and *Pu* at various buoyancy levels. Due to the combined effects of *Re*, *Pu* and Gr_p, the $\overline{Nu}/\overline{Nu}_0$ ratios fall between 0.57 and 10.9 in the present parametric conditions examined. It is noticed that, as the buoyancy interaction improves heat transfer performances, the minimum $\overline{Nu}/\overline{Nu}_0$ ratio of 0.57 is resolved at the zero-buoyancy condition. With the tested Gr_g and Gr_p ranges, the lowest $\overline{Nu}/\overline{Nu}_0$ level detected from the experimental data is 0.82. The systematic variations of $\overline{Nu}/\overline{Nu}_0$ distributions as seen from Fig. 12a–f are the results of ascending buoyancy levels from the zero-buoyancy condition ($Gr_p = Gr_g = 0$). As shown in Fig. 12a that features the zero-buoyancy scenario, the increase of *Pu* at a fixed *Re* incurs the initial reduction in $\overline{Nu}/\overline{Nu}_0$ level when *Re* remains relatively low in the range about $Re < 6000$. Such heat-transfer reductions with $\overline{Nu}/\overline{Nu}_0 < 1$ develop at the parametric regime of low *Re* and low *Pu* as seen in the bottom left corner of Fig. 12a. As *Pu* increases further that leads the parametric condition across this impeding heat transfer regime, the $\overline{Nu}/\overline{Nu}_0$ levels are subsequently recovered and enhanced from the static references. But at the regime with relatively high Reynolds numbers of $Re > 6000$ as shown in Fig. 12a, the $\overline{Nu}/\overline{Nu}_0$ ratios consistently increase with the increase of *Pu*. This interactive *Re*–*Pu* effect acting at the zero-buoyancy condition creates a regime of worst heat transfer scenario as indicated in Fig. 12a within which the $\overline{Nu}/\overline{Nu}_0$ value is reduced to 0.57. In this respect, as the buoyancy impact is vanished due to the zero wall-to-fluid temperature difference, the worse heat transfer regime indicated in Fig. 12a is produced by the weak reciprocation. Further increases of buoyancy level as seen from Fig. 12a → 12b → 12c→ 12d → 12e→ 12f, the spot of worst heat transfer scenario is slightly drifting toward the parametric condition with the higher *Re* and *Pu*. When the buoyancy interactions prevail over the entire flow domain within the tilted static and reciprocating blind tubes, the different degrees of heat transfer impacts between Gr_p on $\overline{Nu}$ and Gr_g on $\overline{Nu}_0$ yield the levels and distributing patterns of $\overline{Nu}/\overline{Nu}_0$ from the zero-buoyancy scenarios as seen in Fig. 12a. It is noticed that the lowest $\overline{Nu}/\overline{Nu}_0$ values at the worst operating conditions as marked in each plot of Fig. 12 gradually increases from 0.57 → 0.76 → 1.01 → 1.02 → 1.06 → 1.08 as $Gr_p(Gr_g)$ systematically increases as shown from 12a → 12f. This particular result infers that the Gr_g effect exerts the less degrees of improving impacts on $\overline{Nu}_0$ than the Gr_p effects on elevating $\overline{Nu}$ values. Accompanying with the elevated worst $\overline{Nu}/\overline{Nu}_0$ ratios by increasing the buoyancy level, the $\overline{Nu}/\overline{Nu}_0$ contour gradually emerges a ripple at the low *Re* regime as $Gr_p(Gr_g)$ systematically increases as displayed from Fig. 12a → f. Such ripple in the $\overline{Nu}/\overline{Nu}_0$ contour as well as the drift of the worst operating spot feature the synergetic *Re*–*Pu*–Gr_p impacts on heat transfer which are well captured by the heat transfer correlations generated. From the viewpoints of design and operation, the worst operating conditions as demonstrated in Fig. 12 are *Re*, *Pu* and Gr_p dependent which require precautions in order to avoid the thermal damages on a moving piston protected by such shaker-bore cooling system.

4. Conclusions

This study experimentally examines the heat transfer performances for a tilted reciprocating anti-gravity open thermosyphon tubes with cooling applications to pistons of marine heavy-duty diesel engine. Several salient points emerge from the data generated as summarized as follows:

1. Relative to the heat transfer references in the vertical static anti-gravity open thermosyphon, the amplified Gr_g effects which improve local and averaged Nu_0 levels along with the elevated Nu_0 values by tilting the blind tube infer the more rigorous vortical circulations in the tilted static anti-gravity open thermosyphon.
2. Alone the line of developing Nu_0 and $\overline{Nu}_0$ correlations, the inter-correlations between *Re* and Gr_g/Re^2 are identified as such that the increase of *Re* amplifies the gravitational buoyancy effect. The zero-buoyancy Nu_0^{ZB} level increases as *Re* increases. A set of heat transfer correlation evaluating $\overline{Nu}_0$ values for the present tilted static anti-gravity open thermosyphon is derived as Eq. (3).
3. Buoyancy interactions in the tilted reciprocating anti-gravity open thermosyphon improve heat transfer performances at both sub-cooled and superheated conditions. Relative to the likewise vertical reciprocating blind tube [17], the higher degree of reciprocating buoyancy impact develops in the tilted reciprocating tube. The complex interactive *Re*, *Pu* and Gr_p effects on *Nu* are observed. Both synergetic *Re* and *Pu* effects amplify the improving buoyancy effects on heat transfer in the tilted reciprocating anti-gravity open thermosyphon.
4. Acting by *Pu* effects alone at fixed *Re*, the zero-buoyancy heat transfer levels (Nu^{ZB}) in the tilted reciprocating blind tube are initially reduced from the static Nu_0^{ZB} references as the reciprocating force remains relatively weak. But the Nu^{ZB} values are soon recovered and enhanced to the levels well above than the static references as *Pu* is further increased. In this respect, the pulsating numbers above which the Nu^{ZB} values become higher than the Nu_0^{ZB} references are systematically reduced as *Re* increases.
5. The derived $\overline{Nu}$ correlation that quantifies the averaged Nusselt numbers along the tilted anti-gravity open thermosyphon tube permits the evaluations of isolated and synergistic impacts of *Re*, *Pu* and Gr_p on *Nu*.
6. Within the parametric ranges examined by this study, the $\overline{Nu}/\overline{Nu}_0$ ratios fall between 0.57-10.9 due to the synergetic *Re*–*Pu*–Gr_p impacts. As $Gr_p(Gr_g)$ systematically increases from zero, the lowest $\overline{Nu}/\overline{Nu}_0$ ratio is accordingly increased with the worst parametric condition drifting toward the higher Reynolds and pulsating numbers. These worst operating conditions along with the lowest $\overline{Nu}/\overline{Nu}_0$ ratios are *Re*, *Pu* and Gr_p dependent which can be successfully identified using the heat transfer correlations generated by this study.

Acknowledgement

This work was funded by the National Science Council, Taiwan, ROC under the Grant No. NSC 91-2611-E-022-003.

References

[1] S.W. Chang, L.M. Su, W.D. Morris, T.-M. Liou, Heat transfer in a smooth-walled reciprocating anti-gravity open thermosyphon, Int. J. Thermal Sci. 42 (2003) 1089–1103.
[2] C.-C. Kao, Experimental study of flow field and heat transfer in a staggered ribbed channel with reciprocating motion, Ms Thesis (2006) Department of Power Mechanical Engineering, National Tsing Hua University, Taiwan, ROC (in Chinese).
[3] G.H.S. Lock, The Tubular Thermosyphon, Oxford Science Publications, Oxford University Press, England, 1992. pp. 286–296.
[4] S.W. Chang, W.D. Morris, T.-M. Liou, S.F. Chiou, Heat transfer in a reciprocating anti-gravity open thermosyphon with two opposite walls roughened by staggered transverse ribs, AIAA J. Thermophys. Heat Tr. 21 (2007) 568–581.
[5] A. Bejian, C.L. Tien, Fully developed natural counterflow in a long horizontal pipe with different end temperatures, Int. J. Heat Mass Tran. 21 (1978) 01–708.
[6] S. Kimura, A. Bejian, Experimental study of natural convection in a horizontal cylinder with different end temperatures, Int. J. Heat Mass Tran. 23 (1980) 1117–1126.

[7] L.C. Fang, D. Nicolaou, J.W. Cleaver, Transient removal of a contaminated fluid from a cavity, Int. J. Heat Fluid Flow 20 (1999) 605–613.
[8] O. Polat, A. Bejian, Laminar natural convection in inclined open shallow cavities, Int. J. Thermal Sci. 41 (2002) 360–368.
[9] Y.L. He, W.Q. Tao, T.S. Zhao, Steady natural convection in a tilted long cylindrical envelop with lateral adiabatic surface, Part 1: theoretical modeling and numerical treatments, Numer. Heat Tran. A 44 (2003) 375–397.
[10] Y.L. He, W.Q. Tao, T.S. Zhao, Z.Q. Chen, Steady natural convection in a tilted long cylindrical envelop with lateral adiabatic surface, Part 2: heat transfer rate, flow patterns and temperature distributions, Numer. Heat Tran. A 44 (2003) 399–431.
[11] E. Bilgen, H. Oztop, Natural convection heat transfer in partially open inclined square cavities, Int. J. Heat Mass Tran. 48 (2005) 1470–1479.
[12] J.F. Hinojosa, G. Alvarez, C.A. Estrada, Three-dimensional numerical simulation of the natural convection in an open tilted cubic cavity, REVISTA MEXICAN DE FÍSICA 52 (2006) 111–119.
[13] B.V. Antohe, J.L. Lage, Experimental investigation on pulsating horizontal heating of a water-filled enclosure, ASME J. Heat Tran. 118 (1996) 889–896.
[14] G.Z. Gershuni, D.V. Lyubimov, Thermal Vibrational Convection, John wiley & Sons, England, 1992.
[15] W.S. Fu, W.J. Shieh, A study of thermal convection in an enclosure induced simultaneously by gravity and vibration, Int. J. Heat Mass Tran. 35 (1992) 1695–1710.
[16] W.S. Fu, W.J. Shieh, Transient thermal convection in an enclosure induced simultaneously by gravity and vibration, Int. J. Heat Mass Tran. 36 (1993) 437–452.
[17] S.W. Chang, L.M. Su, T.L. Yang, S.F. Chiou, Enhanced heat transfer of shaker-bored piston cooling channel with twisted plate, J. Heat Tran. Eng. 28 (2007) 321–334.
[18] Editorial Board of ASME Journal of Heat Transfer, Journal of heat transfer policy on reporting uncertainties in experimental measurements and results, ASME J. Heat Tran. 115 (1993) 5–6.
[19] F.O. Gaa, M. Behnia, G.L. Morrison, Experimental study of flow rates through inclined open thermosyphons, Solar Energy 57 (1996) 401–408.
[20] O. Polat, E. Bilgen, Laminar natural convection in inclined open shallow cavities, Int. J. Thermal Sci. 41 (2002) 360–368.
[21] Y.M. Wang, Experimental study of fluid flow in reciprocating semi-closed cavity, Ms Thesis (2002) Department of Power Mechanical Engineering, National Tsing Hua University, Taiwan, (in Chinese).